

# A DYNAMICAL SYSTEM APPROACH TO MODELING NEURAL NETWORK ACTIVITY IN DROSOPHILA ORIENTATION

S. ISMAIL<sup>1,2</sup>, B. AMBROSIO<sup>1,3</sup>, M.A. AZIZ-ALAOU<sup>1</sup>, AND Y. SOULEIMAN<sup>2</sup>

**ABSTRACT.** We introduce and analyze a class of neural network models motivated by the *Drosophila* central complex, designed to capture the emergence and dynamics of orientation-selective activity bumps. Starting from a biologically inspired ring connectivity model, we derive a simplified reduced model of recurrent neural activity that supports stable localized patterns encoding angular position. We first study the deterministic dynamics and identify parameter regimes ensuring existence and global stability of bump solutions. We then extend the framework to a stochastic setting, incorporating both additive Brownian noise and a Markovian switching mechanism representing time-varying external cues. The resulting system is a switching diffusion with piecewise linear drift, for which we establish well-posedness, characterize the infinitesimal generator, and prove the existence of an invariant measure. Numerical simulations in low and high dimensions illustrate the robustness of the bump attractor under noise and switching stimuli, as well as the convergence toward the predicted stationary states. These results provide a mathematically tractable framework for understanding how population activity in the insect central complex encodes heading direction in the presence of variability.

## 1. INTRODUCTION

This article presents a mathematical description and analysis of neuronal activity in the *Drosophila* ring network. Over the past two decades, experimental studies have established the central role of the *Drosophila* central complex in orientation and navigation during both walking and flight. The central complex comprises the ellipsoid body, the protocerebral bridge, the fan-shaped body, and the noduli.

Individual EPG (E for Ellipsoid Body, P for Protocerebral Bridge, and G for Gall or Glomerulus) neurons exhibit mixed input–output (dendritic) terminals within a single wedge of the ellipsoid body and axonal terminals in a single glomerulus of the protocerebral bridge. During locomotion, the population activity of EPG neurons forms a localized calcium bump in the ellipsoid body, with corresponding representations in the left and right protocerebral bridge. These activity patterns shift coherently across structures, encoding the fly’s angular heading relative to external reference cues (Fig. 1). Key advances were as follows.

The ellipsoid body was first identified as a neural compass encoding heading direction through a ring-shaped activity pattern characterized by a stable, localized bump whose dynamics integrate angular velocity and align with visual landmarks Seelig and Jayaraman [2015]. Green et al. Green et al. [2017] subsequently elucidated the circuit architecture underlying angular path integration in this system, including the protocerebral bridge, thereby providing experimental validation of theoretical models of heading representation. More recently, Cheng et al. ([Cheng et al., 2021]) demonstrated that the central complex performs vector arithmetic by representing heading and movement as sinusoidal population activity in the fan-shaped body, enabling accurate spatial updating when traveling and heading directions diverge, such as during sideways walking. In the present article, we focus on the mathematical properties of a model that provides an efficient and

---

*Date:* April 16, 2026.

*2020 Mathematics Subject Classification.* Primary 92B20; Secondary 34F05.

*Key words and phrases.* Dynamical Systems, Complex Systems, Neuroscience.

Corresponding author: benjamin.ambrosio@univ-lehavre.fr.

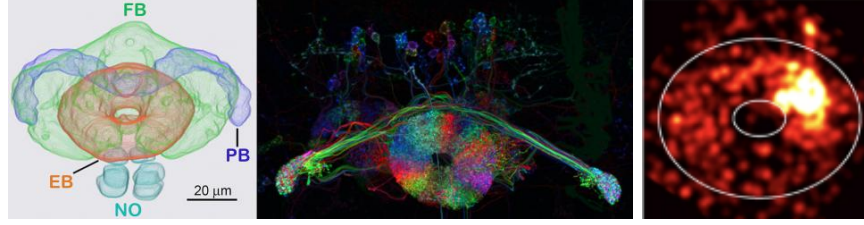


FIGURE 1. Structural, neuronal and functional organization of the central complex. (Left) Schematic reconstruction of major neuropils, including the forebrain (FB), protocerebral bridge (PB), ellipsoid body (EB), and noduli (NO). Scale bar: 20  $\mu\text{m}$ . (Center) Confocal image of multicolor-labeled neurons showing projection patterns and connectivity across central complex regions. (Right) Snapshots of compass-neuron population. Credit: Janelia Research Campus (HHMI); central complex anatomy adapted after Wolff and Rubin [2018] and Kim et al. [2019], CC BY 4.0.

tractable description of calcium-activity bumps in central complex neuronal populations and which can be directly associated with the two-dimensional orientation of the fly. We derive and subsequently provide a rigorous analysis of a simplified version of the ring model described in Kim et al. [2017], Cheng et al. [2021], Abbot [2021], originally introduced in Ben-Yishai et al. [1995], Goldberg et al. [2004] in the context of neuronal activity in the visual cortex.

We consider the following equation:

$$(1) \quad \tau \frac{dr_i}{dt} = -r_i + F \left( \sum_{j=0}^{N-1} A_{ij} r_j + V_i \right) = -r_i + F(x_i),$$

with

$$A_{ij} = J_0 + J_i \cos(\theta_i - \theta_j) + L \cos \left( \theta_i - \theta_j + \frac{\pi}{4} \right) + R \cos \left( \theta_i - \theta_j - \frac{\pi}{4} \right), \quad i \in \{0, \dots, N-1\}.$$

The different terms of the equation can be characterized as follows:

- $r_i = r_i(t)$  is the calcium concentration at angle  $\theta_i$ , with  $\theta_i = i \frac{2\pi}{N}$ .
- $\tau$  is the leakage time scale.
- $A$  is a square matrix representing synaptic interaction strength, with  $A_{ij}$  representing the strength of the connection from angle  $\theta_j$  (or  $\theta_j = j2\pi/N$ ) to angle  $\theta_i$ .
- $V_i = V_i(t)$  is an external input at angle  $\theta_i$ , which may or may not vary over time.
- $x_i = x_i(t) = \sum_{j=0}^{N-1} A_{ij} r_j(t) + V_i(t)$  is the total input at angle  $\theta_i$  over time.
- $F : \mathbb{R} \rightarrow \mathbb{R}$  is a piecewise continuous linear function defined by:

$$(2) \quad F(x) = \begin{cases} x & \text{if } x \geq 0, \\ 0 & \text{otherwise.} \end{cases}$$

In the context of computational neuroscience, it is useful to view model (1) as a closed-form representation of the leaky integrate-and-fire (LIF) model Lapicque [1907], Gerstner and Kistler [2014], Dayan and Abbott [2001], Izhikevich [2007]. We briefly recall here that the leaky integrate-and-fire (LIF) model is a foundational simplification in which a neuron's membrane potential integrates incoming synaptic input while simultaneously decaying (leaking) back toward a resting state, producing a spike whenever a fixed threshold is crossed. Compared to the benchmark Hodgkin-Huxley model Hodgkin and Huxley [1952], this abstraction captures key features of neuronal spiking dynamics while remaining mathematically and computationally tractable, making it widely used in

large-scale neural simulations, such as for example in models of the visual cortex v1 Chariker et al. [2016, 2018]. Here, in (1), the neuron receives excitatory drive from the network when the sum inside  $F$  is positive, while simultaneously undergoing passive decay toward its resting state. Another choice, not considered here would be a  $\tanh$  type function. In order to proceed with the mathematical analysis, we seek to simplify equation (1) while preserving its ability to produce a bump and to represent neuronal activity during the fly's flight. Therefore, we assume that  $J_0 = L = R = 0$ ,  $\tau = 1$ ,  $0 < J_i = \delta > 0$ , so the connectivity matrix  $A$  is therefore reduced to  $A = A_{ij} = \delta \cos(\theta_i - \theta_j)$ . The network model then becomes:

$$(3) \quad \dot{r}(t) = -r(t) + F(Ar(t) + V),$$

where

$$A_{ij} = \delta \cos(\theta_i - \theta_j), \quad i, j \in \{0, \dots, N-1\},$$

and

$$r(t) = \begin{pmatrix} r_0(t) \\ r_1(t) \\ \vdots \\ r_{N-1}(t) \end{pmatrix}, \quad V = \begin{pmatrix} V_0 \\ V_1 \\ \vdots \\ V_{N-1} \end{pmatrix}.$$

Equation (3) is the main equation studied in this article. It describes a network of ordinary differential equations (ODEs), where the number of units  $N$  typically ranges from a few dozen Ishida et al. [2026].

We now introduce a natural stochastic extension of this model. Since it is reasonable to assume that the fly follows a cue while experiencing fluctuations in its motion, we add a Brownian noise term to each component  $r_i$ . We further assume that  $V_i = 0$  everywhere except at a single location representing the cue. Finally, we let the cue evolve according to a continuous-time Markov chain  $I_t$ .

The resulting stochastic differential equation is given by

$$(4) \quad dr_i(t) = \left( -r_i(t) + F\left( \sum_{j=0}^{N-1} A_{ij} r_j(t) + V_i(I_t) \right) \right) dt + \sigma_i dB_i(t),$$

where  $I_t$  is a continuous-time Markov chain on  $\{1, \dots, N\}$  with rate  $\lambda > 0$ . The input vector  $V(I_t)$  is defined such that  $V_j = c > 0$  if  $j = I_t$ , and  $V_j = 0$  otherwise. The remainder of the article is organized as follows. In Section 2, we present the mathematical proofs. We first consider the case  $N = 2$ , and then extend the analysis to the general case. Section 3 is devoted to numerical simulations.

## 2. QUALITATIVE ANALYSIS

In this section, we first study the case  $N = 2$  and then treat the general case.

### 2.1. Qualitative Analysis for the case $N = 2$ .

2.1.1. *Deterministic equation ( $N = 2$ ).* We begin our mathematical analysis with the case  $N = 2$ , for which a more detailed treatment is possible. This simplified setting already captures key features of the system and helps motivate the choice of parameters. Moreover, we restrict our attention to biologically relevant regimes by assuming  $V_1 > 0$ ,  $V_2 = 0$ . Under these assumptions, the deterministic system takes the form of

$$(5) \quad \begin{cases} r_1' &= -r_1 + F(\delta(r_1 - r_2) + V_1), \\ r_2' &= -r_2 + F(\delta(r_2 - r_1)), \end{cases} \quad F(x) = \max(x, 0),$$

where  $\delta > 0$ ,  $V_1 > 0$ . This system models a biological situation in which the fly is exposed to an external stimulus biased toward a preferred direction. As will become clear below, the parameter

regime  $0 < \delta < \frac{1}{2}$  is necessary to ensure biologically meaningful dynamics. The following theorem holds.

**Theorem 2.1.** (i) If  $0 < \delta < \frac{1}{2}$ , equation (5) admits a unique equilibrium

$$E_W = \left( \frac{V_1}{1-\delta}, 0 \right),$$

which is globally asymptotically stable.

(ii) If  $\frac{1}{2} < \delta < 1$ , the system admits two equilibria: a locally stable equilibrium  $E_W$  and a saddle-type coexistence equilibrium  $E_C$ . Every bounded trajectory converges to  $E_W$ .

(iii) If  $\delta > 1$ , the stable equilibrium disappears, the coexistence equilibrium is a saddle, and there exists an open set of initial conditions such that  $|(r_1(t), r_2(t))| \rightarrow \infty$  as  $t \rightarrow \infty$ .

The proof, which consists of a careful but elementary case-by-case analysis, is omitted here. The dynamics are piecewise linear; the nonlinearity only appears when trajectories cross the boundaries separating the regions defined by the argument of the function  $F$ .

2.1.2. *A minimal stochastic process for a two states fly's flight.* Here, we consider the simplest case in dimension two. There are only two opposite directions, and as described above, we add to the ODE a Brownian perturbation together with a random switching mechanism, i.e.,  $(V_1(t), V_2(t))$  alternates randomly between the two states  $(c, 0)$  and  $(0, c)$ , with  $c > 0$ . Formally, let  $Z_t = (X_t, I_t) \in \mathbb{R}^2 \times \{1, 2\}$ , where  $X_t = (r_{1t}, r_{2t})$  solves

$$(6) \quad \begin{cases} dr_{1t} &= \left( -r_1 + F(\delta(r_1 - r_2) + V_1(I_t)) \right) dt + \sigma_1 dB_{1t}, \\ dr_{2t} &= \left( -r_2 + F(\delta(r_2 - r_1) + V_2(I_t)) \right) dt + \sigma_2 dB_{2t}, \end{cases}$$

with  $F(x) = \max(x, 0)$ ,  $B_t = (B_t^1, B_t^2)$  be a two-dimensional Brownian motion. The switching process  $I_t$  is a continuous-time two-state Markov chain with rate  $\lambda > 0$ : when  $I_t = 1$ , we have  $V_1 = c$  and  $V_2 = 0$ , and when  $I_t = 2$ , we have  $V_1 = 0$  and  $V_2 = c$ .

In other words,  $I_t \in \{1, 2\}$  is a continuous-time Markov chain, independent of  $B_t$ , with generator

$$Q = \begin{pmatrix} -\lambda & \lambda \\ \lambda & -\lambda \end{pmatrix}, \quad \lambda > 0.$$

We assume:

$$\delta < 1, \quad \sigma_1, \sigma_2 > 0.$$

For  $i = 1, 2$  define the drift

$$b_i(x) = -x + G(\delta Lx + V^i), \quad x \in \mathbb{R}^2,$$

where  $x = (r_1, r_2)$ ,  $L : \mathbb{R}^2 \rightarrow \mathbb{R}^2$  is linear,  $v_i \in \mathbb{R}^2$ ,  $\delta > 0$ , and  $G((y_1, y_2)) = (F(y_1), F(y_2))$ .

Equation (6) defines a switching diffusion process, a class of systems for which a well-developed theoretical framework is available; see, for instance, Yin and Zhu [2010]. In the present work, however, we emphasize dynamical systems aspects and adopt a semigroup framework. Let

$$P_t f(z) = \mathbb{E}_z[f(Z_t)].$$

The following theorem establishes the well-posedness of (6), shows that  $(P_t)_{t \geq 0}$  defines a semigroup, and provides the existence and explicit characterization of its generator. Let  $C_b$  (resp  $C_b^2$ ) denote the space of continuous (resp. twice continuously differentiable) bounded functions on  $\mathbb{R}^2 \times \{1, 2\}$ .

**Theorem 2.2.** (1) For every initial condition  $(x, i) \in \mathbb{R}^2 \times \{1, 2\}$ , equation (6) admits a path-wise unique continuous solution.

(2) The family  $(P_t)_{t \geq 0}$  defines a strongly continuous semigroup on  $C_b$ . Moreover, for every  $f \in C_b^2$ ,

$$\frac{d}{dt} P_t f = \mathcal{L} P_t f = P_t \mathcal{L} f,$$

where  $\mathcal{L}$  denotes the generator of  $(P_t)$ .

(3) The generator  $\mathcal{L}$  is given, for  $f \in C_b^2$ , by

$$\mathcal{L} f(x, i) = \langle b_i(x), \nabla_x f(x, i) \rangle + \frac{1}{2} \sum_{k=1}^2 \sigma_k^2 \partial_{kk}^2 f(x, i) + \lambda (f(x, j) - f(x, i)), \quad j \neq i.$$

*Proof.* We outline the main steps of the proof, deliberately omitting detailed arguments that follow from standard results. We first remark that for  $a, b \in \mathbb{R}^2$ :

$$|G(a) - G(b)| \leq |a - b|.$$

Since  $L$  is linear, there exists  $C_L > 0$  such that

$$|Lx - Ly| \leq C_L |x - y|.$$

Thus

$$|G(\delta Lx + V^i) - G(\delta Ly + V^i)| \leq |\delta| C_L |x - y|.$$

Therefore

$$|b_i(x) - b_i(y)| \leq |x - y| + |\delta| C_L |x - y| = C |x - y|,$$

for some constant  $C$  independent of  $x, y$ .

Hence  $b_i$  is globally Lipschitz and of linear growth. Between successive switching times of  $I_t$ , the system reduces to a classical SDE of the form

$$dX_t = b_i(X_t) dt + \Sigma dB_t,$$

where  $\Sigma = \text{diag}(\sigma_1, \sigma_2)$ . Since  $b_i$  is globally Lipschitz and  $\Sigma$  is constant, standard results from SDE theory—based, for instance, on a Picard iteration argument (see, e.g., Øksendal [2003], Karatzas and Shreve [1991])—ensure the existence and uniqueness of a continuous solution. Moreover, the Markov chain  $I_t$  has almost surely finitely many jumps on any compact time interval. One can therefore construct the solution pathwise by solving the SDE successively between jump times. Uniqueness on each interval then yields global uniqueness. Next, we prove that,  $P_t$  maps  $C_b$  into itself. First, for boundedness, we remark that

$$|P_t f| = |E[f(Z_t)]| = \left| \int f(z) p_{z_t}(z) dz \right| \leq \|f\|_\infty.$$

where  $p_{z_t}$  denotes the density probability of  $Z(t)$ . Next, let  $X_t^x$  and  $X_t^{x_n}$  denote the solutions of the SDE starting from initial conditions  $x$  and  $x_n$ , respectively. For simplicity, we omit the index  $i$ . The integral formulation of the solutions gives

$$X_t^x = x + \int_0^t b(X_s^x, I_s) ds + \Sigma B_t,$$

$$X_t^{x_n} = x_n + \int_0^t b(X_s^{x_n}, I_s) ds + \Sigma B_t.$$

Subtracting the two equations, we obtain

$$X_t^{x_n} - X_t^x = (x_n - x) + \int_0^t (b(X_s^{x_n}, I_s) - b(X_s^x, I_s)) ds.$$

Since the drift is globally Lipschitz, there exists a constant  $L > 0$  such that

$$|b(x, i) - b(y, i)| \leq L|x - y|$$

for all  $x, y$  and  $i \in \{1, 2\}$ . Therefore

$$|X_t^{x_n} - X_t^x| \leq |x_n - x| + \int_0^t L|X_s^{x_n} - X_s^x| ds.$$

Applying Gronwall's inequality yields

$$|X_t^{x_n} - X_t^x| \leq |x_n - x|e^{Lt}.$$

Taking expectations gives

$$\mathbb{E}|X_t^{x_n} - X_t^x| \leq |x_n - x|e^{Lt}.$$

Hence, if  $x_n \rightarrow x$ , the right-hand side converges to 0, which implies

$$\mathbb{E}|X_t^{x_n} - X_t^x| \rightarrow 0.$$

In particular,

$$X_t^{x_n} \rightarrow X_t^x$$

in probability. Hence, by standard argument, for  $f \in C_b$ ,  $P_t f$  is continuous. Thus  $P_t$  maps  $C_b$  into itself.

Finally, we prove the characterization of the infinitesimal generator. Let  $f \in C_b^2(\mathbb{R}^2 \times \{1, 2\})$  and consider the process  $Z_t = (X_t, I_t)$  with  $X_t = (r_{1t}, r_{2t})$ . Fix  $(x, i)$  and write  $b(x, i) = (b_1(x, i), b_2(x, i))$  for the drift:

$$b_1(x, i) = -x_1 + F(\delta(x_1 - x_2) + V_1(i)), \quad b_2(x, i) = -x_2 + F(\delta(x_2 - x_1) + V_2(i)).$$

We compute the infinitesimal generator  $A$  defined by

$$\mathcal{L}f(x, i) = \lim_{t \rightarrow 0} \frac{P_t f(x, i) - f(x, i)}{t},$$

whenever the limit exists.

Between two switching times of the Markov chain  $I_t$ , the index  $i$  is constant and the process  $X_t$  satisfies the diffusion system

$$dX_t = b(X_t, i) dt + \Sigma dB_t,$$

where  $\Sigma = \text{diag}(\sigma_1, \sigma_2)$ .

Applying Itô's formula to  $f(X_t, i)$  gives

$$df(X_t, i) = \langle b(X_t, i), \nabla_x f(X_t, i) \rangle dt + \frac{1}{2} \sum_{k=1}^2 \sigma_k^2 \partial_{kk}^2 f(X_t, i) dt + \sum_{k=1}^2 \sigma_k \partial_k f(X_t, i) dB_t^k.$$

Taking expectations, the stochastic integral has mean zero, so the expected contribution of the continuous part over a small time interval  $dt$  is

$$\langle b(x, i), \nabla_x f(x, i) \rangle dt + \frac{1}{2} \sum_{k=1}^2 \sigma_k^2 \partial_{kk}^2 f(x, i) dt.$$

The switching process  $I_t$  is a two-state Markov chain with rate  $\lambda$ . Starting from state  $i$ , during a small time interval  $dt$ :

- with probability  $1 - \lambda dt + o(dt)$ , no jump occurs and  $I_t$  remains equal to  $i$ ,
- with probability  $\lambda dt + o(dt)$ , a jump occurs and the state changes to  $j \neq i$ .

If a jump occurs, the value of  $f$  changes from  $f(x, i)$  to  $f(x, j)$ . Therefore the expected increment of  $f$  due to switching is

$$\lambda(f(x, j) - f(x, i))dt + o(dt).$$

Combining the diffusion and switching contributions and dividing by  $dt$ , then letting  $dt \rightarrow 0$ , yields the infinitesimal generator

$$\mathcal{L}f(x, i) = \langle b(x, i), \nabla_x f(x, i) \rangle + \frac{1}{2} \sum_{k=1}^2 \sigma_k^2 \partial_{kk}^2 f(x, i) + \lambda(f(x, j) - f(x, i)), \quad j \neq i.$$

The other details of the proof are omitted here. Another approach is to verify the Hille-Yoshida theorem.  $\square$

Next, we establish the existence and uniqueness of an invariant measure for the process  $Z_t$ .

**Theorem 2.3.** *There exists a unique probability measure  $\pi$  such that*

$$\int P_t f d\pi = \int f d\pi \quad \text{for all } f \in C_b.$$

Furthermore,  $\pi$  satisfies

$$\frac{1}{T} \int_0^T f(Z_t) dt \rightarrow \int f d\pi \quad \text{a.s.}$$

To prove theorem 2.3, we first prove the existence of the measure  $\pi$  in proposition 2.6, uniqueness follows from classical arguments and is omitted. We start with preliminary results.

Define  $\mathcal{V}(x, i) = |x|^2 = r_1^2 + r_2^2$ .

**Lemma 2.4.** *There exist constants  $\alpha > 0$  and  $\beta > 0$  such that*

$$\mathcal{L}\mathcal{V}(x, i) \leq -\alpha\mathcal{V}(x, i) + \beta.$$

Furthermore, one may take any  $\alpha < 2(1 - \delta)$ .

*Proof.* We compute

$$\mathcal{L}\mathcal{V}((r_1, r_2, i) = -2(r_1^2 + r_2^2) + r_1 F(\delta(r_1 - r_2) + V_1(i)) + r_2 F(\delta(r_2 - r_1) + V_2(i)) + \sigma_1^2 + \sigma_2^2.$$

This implies,

$$(7) \quad \mathcal{L}\mathcal{V} \leq -2(1 - \delta - \nu)(r_1^2 + r_2^2) + c \frac{c^2}{8\nu} + \sigma_1^2 + \sigma_2^2.$$

where  $\nu$  can be chosen as small as desired, which yields the result.  $\square$

**Lemma 2.5.** *The following estimate holds,*

$$\mathbb{E}\mathcal{V}(Z_t) \leq e^{-\alpha t} \mathcal{V}(Z_0) + \frac{\beta}{\alpha},$$

hence

$$\sup_{t \geq 0} \mathbb{E}|X_t|^2 < \infty.$$

*Proof.* We first apply Itô's formula to  $d\mathcal{V}$ ,

$$\begin{aligned} d\mathcal{V}(Z_t) &= \frac{\partial \mathcal{V}}{\partial r_1} dr_1 + \frac{\partial \mathcal{V}}{\partial r_2} dr_2 + \frac{1}{2} \frac{\partial^2 \mathcal{V}}{\partial r_1^2} (\sigma_1^2) + \frac{1}{2} \frac{\partial^2 \mathcal{V}}{\partial r_2^2} (\sigma_2^2) \\ &= 2r_1 dr_1 + 2r_2 dr_2 + (\sigma_1^2 + \sigma_2^2) dt \\ &= 2r_1 b_1(r_1, r_2, i) dt + 2r_2 b_2(r_1, r_2, i) dt + (\sigma_1^2 + \sigma_2^2) dt + 2r_1 \sigma_1 dW_1 + 2r_2 \sigma_2 dW_2 \\ &= 2r_1 b_1 + 2r_2 b_2 + \sigma_1^2 + \sigma_2^2 + 2r_1 \sigma_1 dB_1 + 2r_2 \sigma_2 dB_2. \end{aligned}$$

Integrating, between 0 and  $t$ , and taking expectations, we obtain,

$$\mathbb{E}[\mathcal{V}(Z_t)] = \mathcal{V}(Z_0) + \int_0^t \mathbb{E}[\mathcal{L}\mathcal{V}(Z_s)] ds.$$

Using (7) gives

$$\mathbb{E}[\mathcal{V}(Z_t)] \leq \mathcal{V}(Z_0) - \alpha \int_0^t \mathbb{E}[\mathcal{L}V(Z_s)] + \beta t$$

Set

$$u(t) = \mathbb{E}[V(Z_t)],$$

then we have

$$u(t) \leq u(0) - \alpha \int_0^t u(s) ds + \beta t$$

which, thanks to a Gronwall estimate type gives

$$u(t) \leq e^{-\alpha t} u(0) + \frac{\beta}{\alpha} (1 - e^{-\alpha t}).$$

□

We now define empirical measures

$$\mu_T(A) = \frac{1}{T} \int_0^T \mathbb{P}(Z_t \in A) dt.$$

and prove the following convergence result.

**Proposition 2.6** (Existence). *There exists a subsequence  $\mu_{T_k}$  and a measure  $\pi$  such that*

$$\int f d\mu_{T_k} \longrightarrow \int f d\pi \quad \text{for all } f \in C_b.$$

Furthermore,  $\pi$  satisfies:

$$(8) \quad \int P_t f d\pi = \int f d\pi \quad \text{for all } f \in C_b.$$

*Proof.* We first prove that for every  $\varepsilon > 0$  there exists a compact set  $K \subset X$  such that

$$(9) \quad \mu_T(K) \geq 1 - \varepsilon \quad \text{for all } T > 0.$$

For  $R > 0$ ,

$$P(|Z_t| \leq R) = 1 - P(|Z_t| > R)$$

Next we remark that, thanks to the Bienayme-Chebyshev inequality,

$$\mathbb{P}(|X_t| > R) \leq \frac{\mathbb{E}|X_t|^2}{R^2} \leq \frac{C}{R^2}.$$

where the constant  $C$  does not depend on  $t$  nor in  $i$ . We deduce that

$$P(|Z_t| > R) \leq \frac{C}{R^2}.$$

This proves (9). Next, a classical argument (Prokhorov's theorem) proves that there exists a subsequence  $\mu_{T_k}$  and a measure  $\pi$  such that

$$\int f d\mu_{T_k} \longrightarrow \int f d\pi \quad \text{for all } f \in C_b.$$

From the semigroup properties, we deduce that  $\pi$  satisfies (8). Indeed,

$$\int P_t f d\mu_T = \frac{1}{T} \int P_t f(z) \int_0^T p_{z_s} ds dz = \frac{1}{T} \int_0^T \int P_t f(z) p_{z_s} dz ds$$

where  $p_{z_s}$  denotes the density probability of  $Z(s)$ . It follows that

$$\int P_t f d\mu_T = \frac{1}{T} \int_0^T \mathbb{E}[P_t f(Z_s)] ds,$$

$$\begin{aligned}
 &= \frac{1}{T} \int_0^T \mathbb{E}[f(Z_{s+t})] ds, \\
 &= \frac{1}{T} \int_t^{T+t} \mathbb{E}[f(Z_u)] du.
 \end{aligned}$$

Thus,

$$\begin{aligned}
 \int P_t f d\mu_T - \int f d\mu_T &= \frac{1}{T} \int_t^{T+t} \mathbb{E}[f(Z_u)] du - \frac{1}{T} \int_0^T \mathbb{E}[f(Z_u)] du. \\
 &= \frac{1}{T} \left( \int_t^{T+t} \mathbb{E}[f(Z_u)] du - \int_0^T \mathbb{E}[f(Z_u)] du \right), \\
 &= \frac{1}{T} \left( \int_T^{T+t} \mathbb{E}[f(Z_u)] du - \int_0^t \mathbb{E}[f(Z_u)] du \right).
 \end{aligned}$$

Since  $f$  is bounded, we deduce that,

$$\left| \int P_t f d\mu_T - \int f d\mu_T \right| \leq \frac{Ct}{T} \text{ for some constant } C.$$

Letting  $T_k \rightarrow \infty$ , we obtain,

$$\int P_t f d\pi = \int f d\pi.$$

□

*Proof of theorem 2.3.* To prove the theorem, it remains to prove that  $\pi$  is unique. This follows from a standard argument in markov chains theory. We omit the details here and refer to Meyn and Tweedie [2009], Yin and Zhu [2010]. We also deduce that

$$\frac{1}{T} \int_0^T f(Z_t) dt \rightarrow \int f d\pi \quad \text{a.s.}$$

□

**2.2. Qualitative Analysis for  $N \in \mathbb{N}, N > 2$ .** Solutions of Equation (3) can be expressed, for  $t \in (t_k, t_{k+1})$ , as

$$r(t) = e^{B_k(t-t_k)} r(t_k) + \int_{t_k}^t e^{B_k(t-s)} V(s) ds,$$

where  $B_k$  is the matrix associated with the active set of neurons on the interval  $(t_k, t_{k+1})$ .

More precisely, the state space is partitioned according to the regions

$$\mathcal{A}_i = \left\{ r \in \mathbb{R}^N : \sum_{j=0}^{N-1} A_{ij} r_j + V_i > 0 \right\}, \quad i \in \{0, \dots, N-1\}.$$

The subdivision  $t_1, t_2, \dots$  is such that on each interval  $(t_k, t_{k+1})$ , the trajectory remains in a region where the set  $\mathcal{A}(t)$  of active neurons is fixed, that is,

$$\mathcal{A} = \{j \in \{0, \dots, N-1\}; \sum_{j=0}^{N-1} A_{ij} r_j + V_j > 0\}$$

do not change. As long as the trajectory remains within this region, the nonlinearity  $F$  acts linearly, and the dynamics reduce to a linear system with matrix  $B_k$ . We are however proving a more qualitative result. We assume that  $V_0 > 0$  and  $V_i = 0$  for  $i \neq 0$ .

**Proposition 2.7.** *We can rewrite Equation (3) as*

$$(10) \quad r'_i = -r_i + F\left(\delta(m_x \cos \theta_i + m_y \sin \theta_i) + V_i\right),$$

or equivalently,

$$(11) \quad r'_i = -r_i + F\left(\delta R \cos(\theta_i - \phi) + V_i\right),$$

with

$$m_x = \sum_{j=0}^{N-1} r_j \cos \theta_j, \quad m_y = \sum_{j=1}^{N-1} r_j \sin \theta_j,$$

and with  $(R, \phi)$  defined as the polar coordinates of  $m_x + im_y$ ,

$$m_x + im_y = Re^{i\phi}$$

Furthermore, if we assume that

$$\delta < \frac{1}{\sum_{i=1}^{N-1} \sin^2 \theta_i},$$

then,

$$\lim_{t \rightarrow +\infty} m_y = 0$$

and,

$$\forall j \in \{1, \dots, N-1\}, \lim_{t \rightarrow +\infty} r_j - r_{N-j} = 0.$$

*Proof.* We simply apply the formula,

$$\cos(\theta_i - \theta_j) = \cos \theta_i \cos \theta_j + \sin \theta_i \sin \theta_j,$$

therefore

$$\begin{aligned} r'_i &= -r_i + F\left(\delta \sum_j (\cos \theta_i \cos \theta_j + \sin \theta_i \sin \theta_j) r_j + V_i\right) \\ &= -r_i + F\left(\delta (m_x \cos \theta_i + m_y \sin \theta_i) + V_i\right) \\ &= -r_i + F\left(\delta R \cos(\theta_i - \phi) + V_i\right). \end{aligned}$$

Next, we compute  $m'_y$ . We have,

$$\begin{aligned} m'_y &= \sum_{j=1}^{N-1} r'_j \sin \theta_j \\ &= \sum_{j=1}^{N-1} \left( -r_j + F\left(\delta (m_x \cos \theta_j + m_y \sin \theta_j) + V_j\right) \right) \sin \theta_j \\ &= -m_y + \sum_{j>0, j \in \mathcal{A}} \delta (m_x \cos \theta_j \sin \theta_j + m_y \sin^2 \theta_j) \end{aligned}$$

where  $\mathcal{A}$  denotes the active indexes,

$$\mathcal{A} = \{j \in \{0, \dots, N-1\}; \delta (m_x \cos \theta_j + m_y \sin \theta_j) + V_j > 0\}.$$

Now, since

$$\cos \theta_j = \cos \theta_{N-j}, \quad \sin \theta_j = -\sin \theta_{N-j},$$

we obtain,

$$m'_y = -m_y + \delta m_y \sum_{j>0, j \in \mathcal{A}} \sin^2 \theta_j,$$

which proves that if

$$\delta < \frac{1}{\sum_{i=1}^{N-1} \sin^2 \theta_i},$$

$m_y$  converges exponentially toward 0. Finally, we remark that

$$r'_i - r'_{N-i} = -(r_i - r_{N-i}) + 2\delta m_y \sum_{j>0, j \in \mathcal{A}} \sin^2 \theta_j$$

which proves the result since  $m_y$  converges to 0. □

We can now establish the existence of a locally stable bump centered at  $\theta_0 = 0$ .

**Theorem 2.8.** *We assume that*

$$\delta < \min \left\{ \frac{1}{\sum_{\theta_i \in \{-\frac{\pi}{2}, \frac{\pi}{2}\}} \cos^2 \theta_i}, \frac{1}{\sum_{i=1}^{N-1} \sin^2 \theta_i} \right\},$$

then there exists a stationary solution  $\bar{r} = \bar{r}_0, \dots, \bar{r}_{N-1}$  satisfying

$$\bar{r}_0 = \delta m_{\bar{x}} + V_0, \quad \bar{r}_j = \begin{cases} \delta m_{\bar{x}} \cos \theta_j, & \text{if } j > 0 \text{ and } \theta_j \in \{-\frac{\pi}{2}, \frac{\pi}{2}\} \\ 0 & \text{otherwise} \end{cases}$$

with,

$$m_x = \frac{V_0}{1 - \delta \sum_{\theta_i \in \{-\frac{\pi}{2}, \frac{\pi}{2}\}} \cos^2 \theta_i}, \quad m_y = 0.$$

Furthermore,  $\bar{r}$  is locally asymptotically stable in the positive space  $r_j > 0, j \in \{0, \dots, N-1\}$

*Proof.* Under the assumptions, it follows from the proof of proposition 2.7 that  $m'_y = 0$  implies  $m_y = 0$ . Next we compute  $m'_x$ . Adopting the same notations as before, looking for a solution  $m_x > 0$ , we find

$$m'_x = -m_x + \delta m_x \sum_{j \in \mathcal{A}} \cos^2 \theta_j + V_0.$$

Setting  $m'_x = 0$ , we obtain,

$$m_x = \frac{V_0}{1 - \delta \sum_{i \in \mathcal{A}} \cos^2 \theta_i}.$$

Choosing  $\delta$  small enough ensures  $m_x > 0$  and  $\theta_j \in \{\frac{\pi}{2}, \frac{\pi}{2}\} \Leftrightarrow j \in \mathcal{A}$ . The local stability follows from the positive invariance of the spaces  $\mathcal{A}_j, j \in \mathcal{A}$  and  $\mathcal{A}_j^c, j \notin \mathcal{A}$  if  $m_y$  close enough to zero. □

The next section is devoted to numerical simulations.

### 3. NUMERICAL SIMULATIONS

In this section, we present numerical simulations. We begin with the case  $N = 2$ , and then consider a higher-dimensional setting with  $N = 50$ . The simulations were implemented in both C++ and Python; the figures shown here are generated using the Python implementation.

**3.1. Numerical simulations for  $N = 2$ .** In this subsection, we consider equation (6). The system is simulated using the parameter values

$$\delta = 0.2, \quad \sigma_1 = \sigma_2 = 0.1, \quad \lambda = 0.1, \quad c = 1$$

The numerical results are summarized in Figure 2. The top-left panel shows a realization of the Markov switching process  $I(t)$ . The top-right panel displays the trajectories of  $r_1(t)$  and  $r_2(t)$ . The bottom-left panel illustrates the corresponding phase-space trajectory. Finally, the bottom-right panel shows the empirical asymptotic distribution of  $r_1$ . Under this choice of parameters, we observe that the trajectories evolve symmetrically, with the neural activity being high for the neuron driven by the current cue and low for the other, and vice versa when the cue switches. The empirical asymptotic distribution of  $r_1$  exhibits a bimodal structure, with two peaks concentrated near 0 and  $c$  respectively. For this particular realization, we observe a slightly higher mass near 0

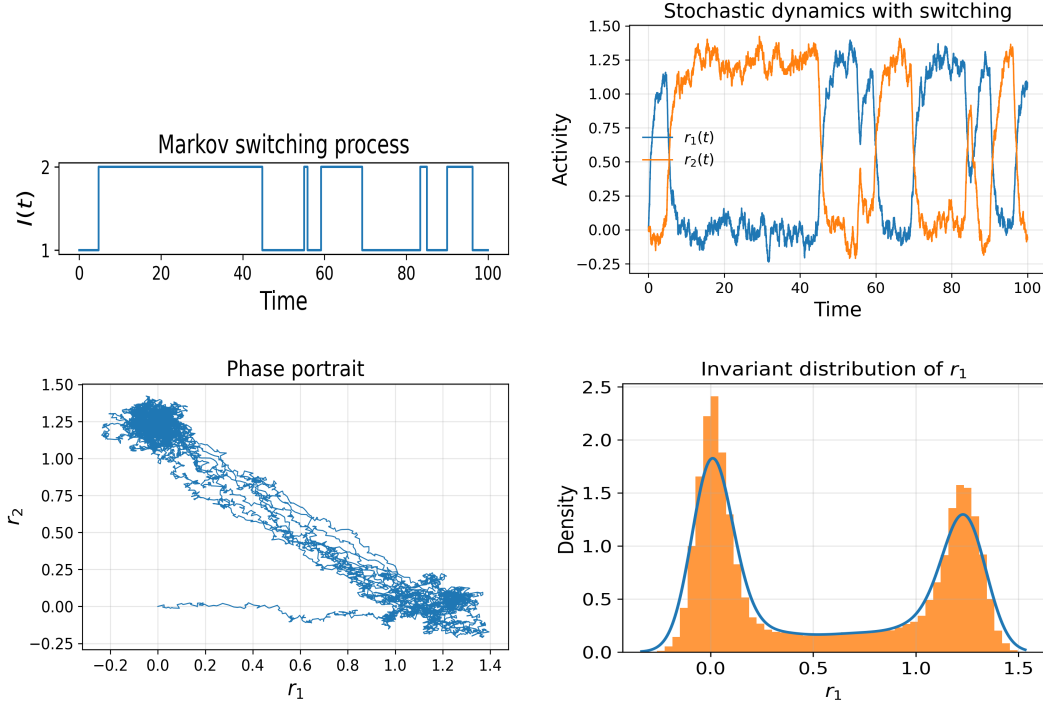


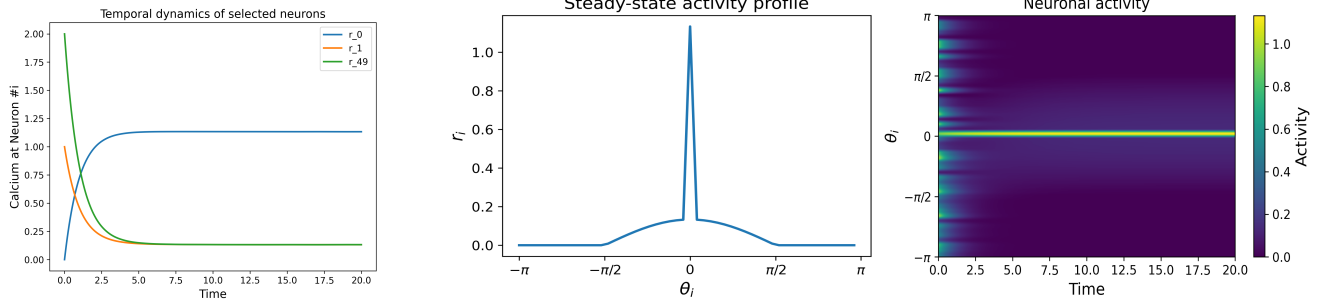
FIGURE 2. Simulations of equation (6) with parameters  $\delta = 0.2$ ,  $\sigma_1 = \sigma_2 = 0.1$ ,  $\lambda = 0.1$ , and  $c = 1$ . The top-left panel shows a realization of the Markov switching process  $I(t)$ . The top-right panel displays the trajectories of  $r_1(t)$  and  $r_2(t)$ . The bottom-left panel shows the corresponding phase-space trajectory. The bottom-right panel illustrates the empirical asymptotic distribution of  $r_1$ . The dynamics exhibit a symmetric switching behavior: neural activity is high for the neuron aligned with the current cue and low for the other, with roles reversing after each switch. The empirical distribution of  $r_1$  is bimodal, with peaks near 0 and  $c$ . In this realization, a slightly higher mass is observed near 0 for  $r_1$  (and correspondingly near  $c$  for  $r_2$ ).

for  $r_1$  (and correspondingly near  $c$  for  $r_2$ ). Overall, these dynamics capture well the behavior of the system, driven by external cues and intrinsic noise, and are consistent with the expected biological response of the fly.

**3.2. Numerical simulations for  $N = 50$ .** In this subsection, we first consider the deterministic network (3) and then the stochastic extension (4) for  $N = 50$ . Figure 3 summarizes the main numerical observations under different initial conditions in the deterministic case. In Panel (A), we show representative time courses for selected indices  $i \in \{0, 1, 49\}$ , starting from a strongly asymmetric initial condition. Despite this imbalance, the system converges toward the stationary profile  $\bar{r}$  identified in Theorem 2.8, with the expected spatial structure  $\bar{r}_i = m_{\bar{x}} \cos(\frac{2\pi i}{50})$ . Panel (B) depicts the asymptotic profile obtained from random initial conditions in  $(0, 1)$ , illustrating convergence toward the same stationary state and its characteristic spatial structure. Finally, Panel (C) presents the full spatio-temporal evolution via a heat map, clearly showing the relaxation toward equilibrium. Finally, figure 4 illustrates the simulation of (4) with the following parameters:

$$\delta = 0.05, \sigma_i = 0.1, \lambda = 0.1, c = 1.$$

The left panel shows the angle  $\theta_i$  corresponding to  $I_t = i + 1 \in \{1, \dots, N\}$  while the right panel presents the full spatio-temporal evolution as a time dependent heat map. Overall, the simulations



(A) Time course for  $i \in \{0, 1, 49\}$ . The following dyssymmetric initial condition was considered  $r_1(0) = 1, r_{49}(0) = 2, r_j(0) = 0$  for  $j \neq 0$ . Asymptotically the trajectory converges toward the stationary solution  $\bar{r}$  from theorem 2.8, with in particular  $\bar{r}_1 = \bar{r}_{49} = m_{\bar{x}} \cos \frac{2\pi}{50}$ .

(B) Asymptotic stationary solution with a bump at 0. Initial conditions were chosen randomly in  $(0, 1)$ . We observe that the solution converges toward the stationary distribution identified in Theorem 2.8.

(C) Same solution as in Panel B, but including time and transient trajectories represented as a heat map. Starting from random initial conditions in  $(0, 1)$ , we observe convergence toward the stationary distribution identified in theorem 2.8.

FIGURE 3. Simulation of equation (3) with  $N = 50$ ,  $\delta = 0.05$  and different initial conditions. We observe that the stationary solution described in theorem 2.8 attracts these initial conditions.

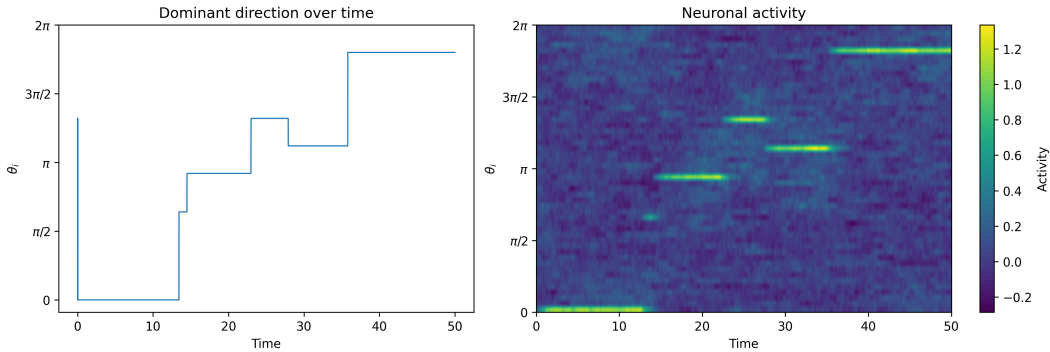


FIGURE 4. Simulation of the network (4) for  $N = 50$  and with  $\delta = 0.05$ ,  $\sigma_i = 0.1$ ,  $\lambda = 0.1$ ,  $c = 1$ . The left panel depicts the angle  $\theta_i$  associated with  $I_t = i + 1 \in \{1, \dots, N\}$ , while the right panel displays the full spatio-temporal evolution in the form of a time-dependent heat map. Overall, the simulations faithfully reproduce the system's behavior under the joint influence of external cues and intrinsic noise, and are consistent with the expected biological response of the fly across all directions.

accurately capture the system's behavior under the combined effect of external cues and intrinsic noise, and are consistent with the expected biological response of the fly across all directions.

#### 4. CONCLUSION

In this article, we have introduced and analysed a family of stochastic and deterministic neural field models inspired by the ellipsoid body's architecture of the *Drosophila* central complex. Starting from a biologically motivated connectivity structure, we derived a reduced tractable model capable of sustaining localized activity bumps and encoding angular information. We provided a mathematical analysis of both the deterministic and stochastic dynamics. In particular, we established well-posedness, characterized the generator of the associated switching diffusion, and proved the existence of a stationary regime. In the deterministic setting, we identified parameter regimes

ensuring global convergence toward a stable bump solution. In the stochastic case, we showed that the interplay between noise and external cues preserves the qualitative structure of the dynamics while inducing realistic switching and variability in neural activity. From a biological perspective, these results contribute to the ongoing effort to understand how low-dimensional population codes emerge from recurrent neural circuits in the insect brain. The *Drosophila* central complex is currently an active area of experimental and theoretical research, and increasingly detailed connectomic data continue to refine our understanding of its functional architecture. Our work provides a mathematically grounded framework that can be extended to incorporate more realistic connectivity patterns and sensory inputs, and may serve as a basis for future studies linking circuit-level mechanisms to navigation and decision-making in biological systems.

## REFERENCES

- L. Abbot. Neuroscience lecture. <https://www.youtube.com/watch?v=K-uMBbt5e5c&t=2089s>, 2021. Accessed online April 12 2026.
- R. Ben-Yishai, R. Lev Bar-or, and H. Sompolinsky. Neurobiology. *Proc. Natl. Acad. Sci. USA*, 92: 3844–3848, 1995.
- L. Chariker, R. Shapley, and L-S. Young. Orientation selectivity from very sparse lgn inputs in a comprehensive model of macaque v1 cortex. *Journal of Neuroscience*, 36(49):12368–12384, 2016.
- L. Chariker, R. Shapley, and L-S. Young. Rhythm and synchrony in a cortical network model. *Journal of Neuroscience*, 38(40):8621–8634, 2018.
- L. Cheng, L. F. Abbott, and M. Gaby. Building an allocentric travelling direction signal via vector computation. *Nature*, 2021.
- Peter Dayan and L. F. Abbott. *Theoretical Neuroscience: Computational and Mathematical Modeling of Neural Systems*. MIT Press, 2001.
- Wulfram Gerstner and Werner M. Kistler. *Spiking Neuron Models: Single Neurons, Populations, Plasticity*. Cambridge University Press, 2nd edition, 2014.
- Joshua A. Goldberg, Uri Rokni, and Haim Sompolinsky. Patterns of ongoing activity and the functional architecture of the primary visual cortex. *Neuron*, 42(3):489–500, 2004. ISSN 0896-6273. doi: [https://doi.org/10.1016/S0896-6273\(04\)00197-7](https://doi.org/10.1016/S0896-6273(04)00197-7). URL <https://www.sciencedirect.com/science/article/pii/S0896627304001977>.
- J. Green, A. Adachi, K. K. Shah, J. D. Hirokawa, P. S. Magani, and G. Maimon. A neural circuit architecture for angular integration in *Drosophila*. *Nature*, 546(7656):101–106, 2017.
- Alan L. Hodgkin and Andrew F. Huxley. A quantitative description of membrane current and its application to conduction and excitation in nerve. *The Journal of Physiology*, 117(4):500–544, 1952.
- Itzel G. Ishida, Sachin Sethi, Thomas L. Mohren, Mia K. Haraguchi, L.F. Abbott, and Gaby Maimon. Neuronal calcium spikes enable vector inversion in the *drosophila* brain. *Cell*, 189: 748–764, 2026.
- Eugene M. Izhikevich. *Dynamical Systems in Neuroscience: The Geometry of Excitability and Bursting*. MIT Press, 2007.
- Ioannis Karatzas and Steven Shreve. *Brownian Motion and Stochastic Calculus*, volume 113 of *Graduate Texts in Mathematics*. Springer, 2 edition, 1991.
- S. S. Kim, H. Rouault, S. Druckmann, and V. Jayaraman. Ring attractor dynamics in the *Drosophila* central brain. *Science*, 2017.
- Sung Soo Kim, Ann M. Hermundstad, Sandro Romani, L. F. Abbott, and Vivek Jayaraman. Generation of stable heading representations in diverse visual scenes. *Nature*, 576:126–131, 2019. doi: 10.1038/s41586-019-1767-1.
- Louis Lapicque. Recherches quantitatives sur l’excitation électrique des nerfs traitée comme une polarisation. *Journal de Physiologie et de Pathologie Générale*, 9:620–635, 1907.

- S.P. Meyn and R.L. Tweedie. *Markov Chains and Stochastic Stability*. Cambridge University Press, 2009.
- Bernt Øksendal. *Stochastic Differential Equations: An Introduction with Applications*. Springer, Berlin, 6 edition, 2003.
- J. D. Seelig and V. Jayaraman. Neural dynamics for landmark orientation and angular path integration. *Nature*, 521:186–191, 2015.
- Torben Wolff and Gerald M. Rubin. Neuroarchitecture of the drosophila central complex: A catalog of nodulus and asymmetrical body neurons and a revision of the protocerebral bridge catalog. *Journal of Comparative Neurology*, 526(16):2585–2611, 2018. doi: 10.1002/cne.24512.
- George Yin and Chao Zhu. *Hybrid Switching Diffusions: Properties and Applications*, volume 63 of *Stochastic Modelling and Applied Probability*. Springer, 2010. doi: 10.1007/978-1-4419-1105-6.

1.NORMANDIE UNIV., LMAH UR 3821, 25 RUE PHILIPPE LEBON, LE HAVRE, 76600, NORMANDIE, FRANCE

2.UNIVERSITY OF DJIBOUTI, DJIBOUTI

3.THE HUDSON SCHOOL OF MATHEMATICS, 244 FIFTH AVENUE, NEW YORK, 10001, NEW YORK, USA  
*Email address:* `benjamin.ambrosio@univ-lehavre.fr`